Errors In Inverse Problem Solutions Due To Inaccuracies In Torso and Cardiac Anatomy

R. Martin Arthur, PhD and Scott B. Marrus, MD/PhD
Electrical & Systems Engineering, Washington University in St. Louis, St. Louis, MO 63130
Email: rma@ese.wustl.edu

***Abstract*—Electrocardiographic imaging, i.e., noninvasive determination of cardiac sources based on body-surface maps using individualized heart and torso models can assess cardiac conditions. As the tools for rapidly acquiring individualized heart and torso models become more common, it is important to assess the effect of errors in those models on the quality of ECG images. Images of the Visible Human Male were segmented to create full-body and heart-model surfaces, along with truncated torso models. REs of inverse solutions increased by 33% at the peak of the R wave and by 24% over the QRS complex for typical torso models compared to the full body. To quantify effects of heart location on inferred activation time (AT) and activation-recovery intervals (ARI), the heart location was shifted within the torso. Reconstructed AT and ARI maps demonstrated that overall patterns were relatively preserved despite shifts in the x- and y-axes, but suffered significant degradation after shifts in the z-axis (towards the head). Results suggest that fidelity of torso-surface construction near the heart and the location of the heart in the z-direction are critical steps in inverse-problem solutions.**

Keywords—inverse electrocardiography, heart torso models, Tikhonov regularization, epicardial potentials, activation, recovery.

I. Introduction

Normal cardiac function depends on coordinated mechanical and electrical function[1]. Precisely coordinated myocyte depolarization and repolarization is required for efficient mechanical function and, conversely, abnormal mechanical function alters cellular electrical properties. This interplay of mechanical and electrical properties is particularly relevant in heart failure, which involves both mechanical pump failure and a significant risk of malignant arrhythmias and sudden cardiac death.

Both mechanistic studies and clinical management are limited, however, by the lack of a bedside imaging modality providing both high-resolution electrical imaging and functional, mechanical information. Several modalities provide cardiac structural and mechanical information, including computed tomography, magnetic resonance imaging, and ultrasound.

Ultrasound remains the mainstay of clinical cardiac imaging due to the combination of convenient bedside usage, real-time imaging, detailed functional information and tissue characterization[2]. In contrast, the electrocardiogram, lacking significant spatial resolution, remains the primary clinical tool for the assessment of electrical function. Previous work has demonstrated the feasibility of solving the inverse problem to reconstruct epicardial electrical activity based on body surface potential mapping and the anatomic relationship of the torso surface and the epicardium[3].

The accuracy of heart and torso models clearly affects the quality of solutions to the forward and inverse problems of electrocardiography. Although a given geometric error in a heart model, presumably has more adverse effect on inverse solutions than the same error in torso geometry, we show that torso model formation can have a significant effect on inverse-solution errors.

Noninvasive determination of cardiac sources based on body-surface maps using individualized heart and torso models can assess cardiac conditions more fully and more accurately than standard 12-lead analysis[3–6]. As the tools for rapidly acquiring individualized heart and torso models become more common, it is important to assess the efficacy of inverse methods that can be applied in a clinical, rather than a research setting, and in particular, to delineate the necessary accuracy with which torso and cardiac anatomies are described..

Here we report effects on inverse solutions in a simulated systematic reduction of a full-body surface to a torso model by truncating anatomical features[7]. We also describe effects on activation and recovery times derived from inverse solutions from measurements in an adult male, whose inferred cardiac potentials were previously reported[3].

II. Methods

Both the simulation study of torso effects and the human study used to determine effects of heart location inaccuracy on activation and recovery were based on conventional zero-order Tiknov inverse solutions for cardiac potentials.

A. Inverse-Problem Solutions

Heart-surface potentials were inferred using Tikhonov regularization[8].

$$\hat{\Phi}_H \;=\; (Z_{BH}^t\, Z_{BH} \;+\; \tau \mathbf{I})^{-1}\; Z_{BH}^t\; (\Phi_B + \Phi_N) \quad , \qquad (1)$$

where $\mathbf{I}$ is the identity matrix (zero-order) and Φ_N, the noise in the surface potentials, Φ_B.

To solve the forward-problem, i.e., to find body-surface potentials Φ_B from heart-surface potentials Φ_H, transfer-coefficients Z_{BH} were calculated for the heart surface to the nodes of all body surfaces using the method of Barr and coworkers[9].

$$\Phi_B \;=\; Z_{BH}\; \Phi_H \quad . \qquad (2)$$

B. Torso Model Effects on Cardiac Potentials

Torso construction effects were simulated from heart and full-body models based on manual segmentation of parallel color images of the Visible Human Male[10], as shown in Fig. 1. This approach allowed for body-surface truncation without affecting the location of remaining model nodes or electrode locations, so that inverse solutions could be compared at the same electrode sites. Body-surface potentials were calculated using measured heart-surface potentials from the ventricles of an adult male[11].

To generate full-body and truncated torso models for comparison, we segmented color images of the Visible Human Male[10] in 1-cm steps from head to toe. Specifically, the surface of the head and neck, heart, torso, pelvis, arms and legs were sampled on contours separated by 1 cm.

These contours were resampled at uniform intervals along each contour. The uniform-interval samples were upsampled to be sure spatial aliasing had not occurred during resampling. Surfaces were formed by triangulating between contours. The heart of the Visible Human Male was also segmented at 1-cm intervals to form the 93-node heart surface heart model shown in Fig. 1.

The full-body surface was systematically reduced by removing 1) the legs, then 2) the right arm, 3) the left arm, 4) the pelvis, head and neck, and 5) the shoulders to form the torso models shown in Fig. 1. Positions of 163 simulated electrode locations are also shown in Fig. 1. They were at the same positions in all truncated torso models as they were on the full-body model. All models had closed surfaces and subtended a solid angle of 4π, as expected.

Body-surface potentials Φ_B were calculated at the electrode locations in the full-body and all torso models for unit voltages, i.e., $\Phi_H = [\mathbf{1}]$. Φ_N was set to $10\mu v$ peak-to-peak[12]. Because Φ_H was known, an optimal value for the regularization parameter τ was found.

Time varying values for Φ_B were found using known heart-surface potentials Φ_H, taken from 90-electrode sock recordings in an adult male during normal sinus rhythm over the QRS complex using intraoperative mapping techniques[13]. These sock-electrode recordings, acquired from patients undergoing arrhythmia surgery for sustained monomorphic ventricular tachycardia, were mapped to the heart model using methods described previously[11].

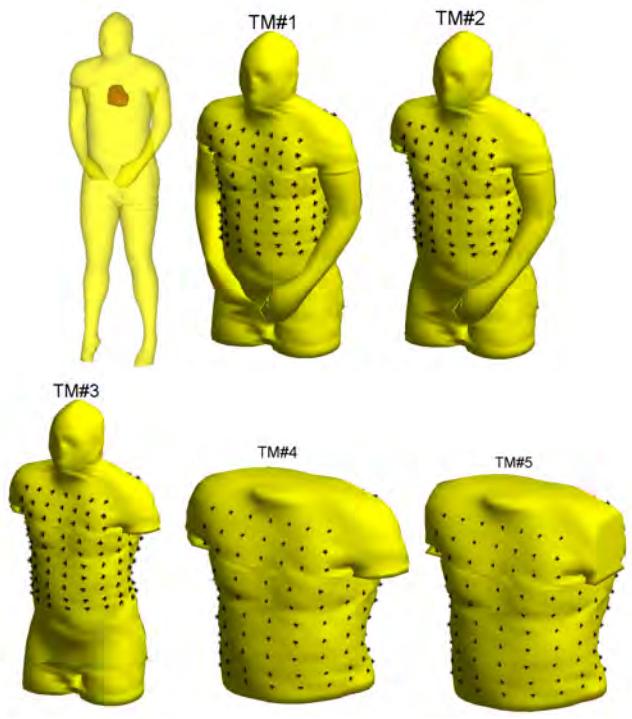

Fig. 1. Torso models reduced from the full surface of the Visible Human Male shown in the upper left panel. TM#1 is the full body without legs. TM#2 is without legs and the right arm. TM#3 is without legs and arms. TM#4 is without legs, pelvis, arms, head and neck. TM#5 is without legs, pelvis, arms, head, neck and shoulders. All models show the location of simulated electrode sites (asterisks) used in both forward and inverse solutions.

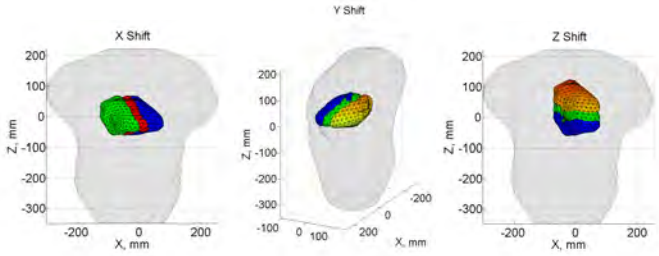

Fig. 2. Simulations of errors in heart location. The original heart location is in blue. It was shifted by up to 50 mm in each direction. The X location was shifted to the right (negative direction). The Y location was shifted towards the back (positive direction). The Z location was shifted upwards (positive direction).

C. Heart Location Effects on AT and ARI

Studies of the effects of heart location inaccuracy were based on measurements in an adult male, whose inverse solutions were reported previously[3]. Solutions for activation time (AT) and activation-recovery interval (ARI) on the 314-node heart were derived from those solution for the heart at its original location and at shifted positions.[2]. The heart was shifted by 5, 10, 20 and 50 mm in the X, Y and Z directions. The X shift was to the right (negative); Y shift was to the back (positive); the Z shift was towards the head (positive).

Activation time (AT) for each node was defined as the time of minimal dV/dt during the QRS complex; RT for each node was determined using the traditional Wyatt method (the time of maximal dV/dt during the local T wave)[14]. The activation-recovery interval (ARI) was calculated for each node as the difference between AT and RT at that node.

D. Relative Error (RE)

Each inverse solution in the torso-simulation study was optimized with a value for τ in Eq. 1 that minimized relative error (RE) at each instant during the QRS complex.

$$RE(t_i) = \sqrt{\frac{(\mathbf{\Phi}^c_H(t_i) - \mathbf{\Phi}^i_H(t_i))^*(\mathbf{\Phi}^c_H(t_i) - \mathbf{\Phi}^i_H(t_i))}{\mathbf{\Phi}^c_H(t_i)^*\mathbf{\Phi}^c_H(t_i)}} \quad , \tag{3}$$

where $RE(t_i)$ is the relative error calculated at time t_i, $\mathbf{\Phi}_H^c(t_i)$ is a vector representing the correct (known) potentials on the heart surface at time t_i, and $\mathbf{\Phi}_H^i(t_i)$ is a vector representing the inferred potentials. The RE reported for each inverse solution was the mean of 10 runs. RE and correlation coefficient (CC) were used the quantify the changes in AT and ARI maps.

III. Results

Effects of model formation via full-body truncation on inverse-problem solutions were quantified using relative errors (REs) in the inferred potentials $\hat{\Phi}_H$. RE and CC were used the quantify changes in AT and ARI maps with heart displacement.

A. Effect of Torso Truncation on Inferred Cardiac Potentials

REs of inverse solutions near the peak of the R wave and over the QRS complex with $10\mu v$ peak-to-peak noise added to body-surface potentials at all 163 electrode sites are given in Table I for all of the torso models. The RE at the peak of the R wave increased by 33% and by 24% over the QRS complex in TM#4 and TM#5 (see Fig. 1 & Table I). These models are typical of the models used in inverse electrocardiography.

	Full-Body	TM#1	TM#2	TM#3	TM#4	TM#5
R Wave Peak	0.36	0.36	0.47	0.48	0.48	0.48
$TM_i : Full$		1.00:1	1.31:1	1.33:1	1.33:1	1.33:1
QRS Complex	0.45	0.45	0.53	0.55	0.56	0.56
$TM_i : Full$		1.00:1	1.18:1	1.22:1	1.24:1	1.24:1

TABLE I. Relative Error of Cardiac Potential Solutions with $10\mu v$ peak-to-peak Noise

B. Effect of Heart Shift on AT and ARI

AT in the original heart location, along with AT after shifting the heart by 5 mm is given in Fig. 3. ARI in the original heart location, along with ARI after shifting the heart by 5 mm is given in Figs 4. Changes in AT and ARI are quantified in Fig. 5, which plots RE and CC for shifts of 5, 10, 20 and 50 mm.

IV. Discussion

Torso and heart model construction practices vary considerably[6,15]. Models have usually been based on segmenting contours from images, such as CT or MRI scans. It is becoming more common, however, to build models from point clouds[3,16]. Whatever the method, there remains the problem of selecting anatomical features to use in constructing models that minimize errors in inferred cardiac sources.

Although the forward-problem errors due to torso-model truncation were only 1-3%, the effect of torso-model truncation on the inverse was an order of magnitude greater, 20-30% (Table I). Most of this increase occurred with the removal of the arms, especially the left arm. RE did not significantly increase with the additional removal of head, pelvis, and shoulders.

These findings suggest that, in addition to the need for individualizing torso models shown previously[11], care must be taken in the process of extracting the torso model from the full body for each subject. The spatial distribution for the forward-problem REs showed that it was largest on the left

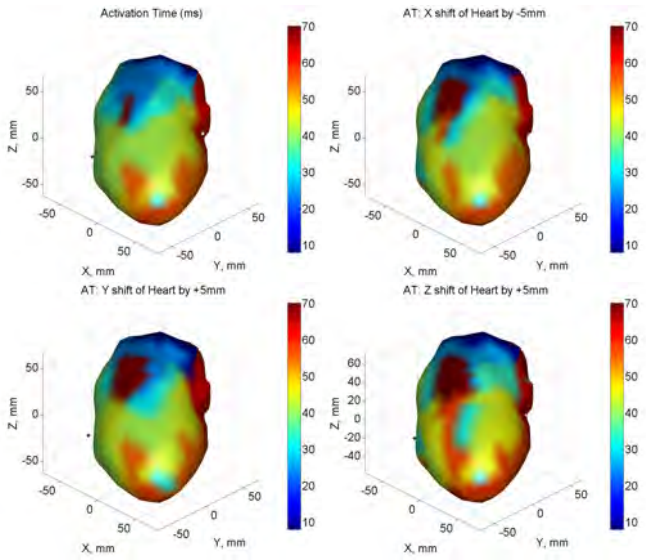

Fig. 3. Changes in Activation Time caused by 5 mm shifts in heart position. The original AT map is in the upper left panel. Pattern changes versus distance are quantified in Fig. 5.

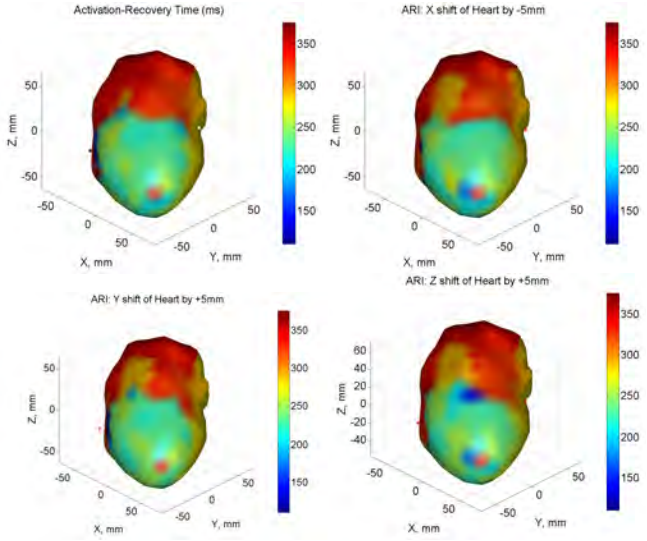

Fig. 4. Changes in Activation-Recovery Times caused by 5 mm shifts in heart position. The original ARI map is in the upper left panel. Pattern changes versus distance are quantified in Fig. 5.

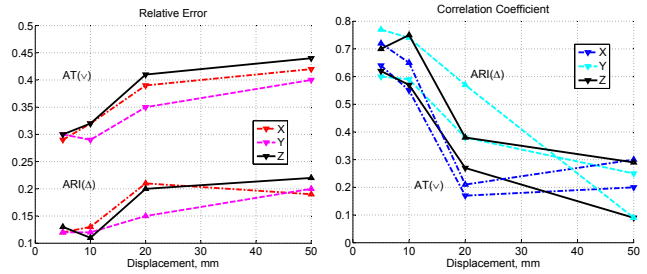

Fig. 5. Relative Errors and Correlation Coefficients with heart displacement for Activation Time (AT) and Activation-Recovery Interval (ARI) .

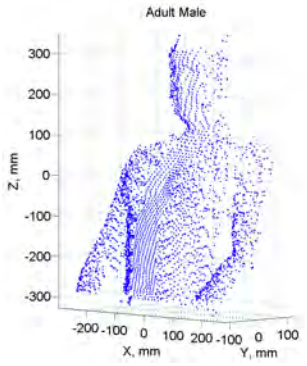

Fig. 6. Kinect sensor[17] mapping of the anterior surface of an adult male. Anatomic detail in the region of the heart and left arm suitable for refining the torso model in that region to reduce forward-inverse solution errors.

side at the bottom of the torso, in the vicinity of the heart, and on the upper left back. These results suggest that, in these areas, a torso model should closely match a given individual's torso.

The Visible Human Male measurements were used to create zonal models, that is, they were constructed from adjacent, sampled contours. It may not be possible or desirable, however, to construct a torso model from contours. More commonly now, a point cloud is used to build a torso model[16]. Because of the relative ease of forming a point cloud with inexpensive 3D sensors, such as the Kinect[17], torso models built from clouds can more readily retain torso detail in the vicinity of the heart, including more of the arms (See Fig. 6).

Displacement of the heart position by more than 20 mm resulted in a RE of 40% for AT and 20% for ARI (Fig. 5). However, visual inspection of the patterns, as would likely be the clinical usage of this data, reveals that the overall pattern of AT and ARI remain largely unchanged after displacements of up to 50 mm in the x-axis and y-axis but are significantly altered by as little as 5 mm displacement in the z-axis. In Figs. 3 and 4, note the greater effect of z-axis displacement. This result highlights the importance of accurate localization of the heart position, particularly in the z-axis.

This study suggests that modeling the torso surface in the vicinity of the heart and near regions where the full body is truncated to form the torso model, along with accurate location of the heart model in the z-directions have the greatest impact on inverse-problem errors.

V. Conclusions

Electrocardiographic imaging can assess cardiac conditions, but is limited by errors in inverse solutions due to inaccuracies in torso and cardiac anatomy. Torso model construction produced an increase in RE of cardiac potentials of 20-30% compared to the full-body inverse. Most of this increase in RE occurred with removal of the arms, especially the left arm. Although errors of up to 50 mm in heart location were tolerable in the x- and y-axis cardiac position (in terms of overall AT and ARI patterns), errors of 5 mm in z-axis resulted in significant degradation of the AT and ARI patterns. Results suggest that fidelity of torso-surface construction near the heart and heart location, especially along the z-axis are critical steps in inverse-problem formation.

References

[1] E. Pfeiffer, J. Tangney, J. Omens, and A. McCulloch, "Biomechanics of cardiac electromechanical coupling and mechanoelectric feedback," *J Biomechanical Engr*, vol. 136, pp. 1–11, 2014.

[2] S. Marrus, C. Andrews, D. Cooper, M. Faddis, and Y. Rudy, "Repolarization changes underlying long-term cardiac memory due to right ventricular pacing: Noninvasive mapping with ecgi," *Circ Arrhyth Electrophysiol*, vol. 5, no. 4, pp. 773–781, 2012.

[3] R. Arthur and J. Trobaugh, "Electrocardiographic textbooks based on template hearts warped using ultrasonic images," *IEEE Trans on Biomed Engr*, vol. 59, no. 9, pp. 2531–2537, 2012.

[4] R. Arthur, S. Wang, and J. Trobaugh, "Changes in body-surface electrocardiograms from geometric remodeling with obesity," *IEEE Trans on Biomed Engr*, vol. 58, no. 6, pp. 1565–1573, 2011.

[5] Y. Wang, P. Cuculich, J. Zhang, K. Desouza, R. Vijayakumar, J. Chen, M. Faddis, B. Lindsay, T. Smith, and Y. Rudy, "Noninvasive electroanatomic mapping of human ventricular arrhythmias with electrocardiographic imaging," *Sci Transl Med*, vol. 3, p. 98ra84, 2011.

[6] A. van Oosterom, "The inverse problem of bioelectricity: an evaluation," *Med Biol Eng Comput*, vol. 50, no. 9, pp. 891–902, Sept 2012.

[7] R. Arthur, K. Timbadia, A. Rauf, and J. Trobaugh, "Effects of reducing the full-body surface to a torso model in forward and inverse electrocardiography," *International J of Bioelectromagnetism*, vol. 5, pp. 312–313, 2003.

[8] D. Beetner and R. Arthur, "Estimation of heart-surface potentials using regularized multipole sources," *IEEE Trans on Biomed Engr*, vol. 51, pp. 1366–1373, 2004.

[9] R. Barr, M. Ramsey, III, and M. Spach, "Relating epicardial to body surface potential distributions by means of transfer coefficients based on geometry measurements," *IEEE Trans on Biomed Engr*, vol. BME-24, pp. 1–11, 1977.

[10] V. Spitzer, M. Ackerman, A. Scherzinger, and D. Whitlock, "The visible human male: A technical report," *J Am Med Inform Assoc*, vol. 3, pp. 118–130, 1996.

[11] R. Arthur, D. Beetner, H. Ambos, and M. Cain, "Improved estimation of pericardial potentials from body-surface maps using individualized torso models," *J of Electrocardiology*, vol. 31 (supplement), pp. 106–113, 1998.

[12] R. Arthur, "Signal quality of resting electrocardiograms," *J of Electrocardiology*, vol. 16, no. 3, pp. 235–244, 1983.

[13] C. Rokkas, T. Nitta, R. Schuessler, B. Branham, M. Cain, J. Boineau, and J. Cox, "Human ventricular tachycardia: Precise intraoperative localization with potential distribution mapping," *Annals of Thoracic Surgery*, vol. 57, pp. 1628–1635, 1994.

[14] C. Haws and R. Lux, "Correlation between *in vivo* transmembrane action potential durations and activation-recovery intervals from electrograms. effects of interventions that alter repolarization time," *Circulation*, vol. 81, pp. 281–288, 1990.

[15] W. Smith, "Direct mapping of bioelectric activity," *Critical Reviews in Biomedical Engineering*, vol. 27, pp. 339–358, 1999.

[16] S. Lodka and R. Franke, "Scattered data techniques for surfaces," in *Proceedings Dagstuhl '97, Scientific Visualization*, G. N. H Hagen and F. Post, Eds., vol. IEEE No PR00503. IEEE Computer Society, 1999, pp. 1–42.

[17] K. Khoshelham and S. Elberink, "Accuracy and resolution of kinect depth data for indoor mapping applications," *Sensors*, vol. 12, no. 2, pp. 1437–1454, 2012. [Online]. Available: http://www.mdpi.com/1424-8220/12/2/1437